www.czasopisma.pan.pl PAN www.journals.pan.pl
Opto-Electronics Review 26 (2018) 50–56

Contents lists available at ScienceDirect

Opto-Electronics Review

journal homepage: http://www.journals.elsevier.com/opto-electronics review

A high-sensitivity photonic crystal fiber (PCF) based on the surface plasmon resonance (SPR) biosensor for detection of density alteration in non-physiological cells (DANCE)

F. Wang [a], Z. Sun [a,*], C. Liu [b,*], T. Sun [c], P.K. Chu [d]

[a] Institute of Materials Processing and Intelligent Manufacturing & Center for Biomedical Materials and Engineering, Harbin Engineering University, Harbin 150001, China
[b] School of Electronics Science, Northeast Petroleum University, Daqing 163318, China
[c] Institute of Microelectronics, Agency of Science, Technology and Research (A*STAR), 117685, Singapore
[d] Department of Physics and Materials Science, City University of Hong Kong, Tat Chee Avenue, Kowloon, Hong Kong, China

ARTICLE INFO

Article history:
Received 28 July 2017
Received in revised form 8 December 2017
Accepted 5 January 2018
Available online 6 February 2018

Keywords:
PCF-SPR biosensor
DNACE
Sensitivity
Resolution

ABSTRACT

A highly sensitive photonic crystal fiber based on the surface plasmon resonance (PCF-SPR) biosensor for the detection of the density alteration in non-physiological cells (DANCE) is described. Human acute leukemia cells are determined by the discontinuous sucrose gradient centrifugation (DSGC) in which the cells are separated into several bands. The separated cells with different intracellular densities and refractive indexes (RI) ranging from 1.3342 to 1.3344 are distinguished *in situ* by means of the differential transmission spectrum. The biosensor shows a maximum amplitude sensitivity of 2000 nm/RIU and resolution as high as 5×10^{-5} RIU. According to the wavelength interrogation method, a maximum spectral sensitivity of 9000 nm/RIU in the sensing range between 1.33 and 1.53 is achieved, corresponding to a resolution as high as 1.11×10^{-5} RIU for the biosensor. The proposed PCF-SPR biosensor has promising application in biological and biochemical detection.

1. Introduction

Surface plasmon resonance (SPR), an optical biosensing technique, is a highly sensitive, real-time, and label-free approach to study biomolecular interactions [1]. The SPR method is based on optical measurement of refractive index changes associated with the binding of analyte molecules in a sample to recognize molecules immobilized on the SPR sensor [2]. They have been increasingly applied to the detection of chemical and biological substances in important areas such as medical diagnostics, environmental monitoring, food safety, and security [3,4]. Since late 1990's, SPR biosensors have become the main tools for the study of biomolecular interactions both in life science and pharmaceutical research [5]. SPR biosensors have been successfully applied to a wide variety of biological molecules with different sizes, such as small molecules, Mr <500 Da [6], to larger and more complex structures including proteins, nucleotides, viruses, and peptides with therapeutic potential in recent years [7–11]. However, the conventional SPR configuration is bulky and not suitable for remote sensing consequently limiting large scale fabrication for real time applications [12]. To overcome this limitation, the feasibility of fiber-based SPR sensors in sensing applications has been explored [13]. In 2006, L. Rindorf *et al.* proposed SPR biochemical sensors of long-period gratings based on PCF and analyzed design principles with a monolayer of poly-L-lysine and double-stranded DNA in biosensing applications [14]. The simulation results indicated that a refractive-index resolution of 10^{-4}RIU was obtained from the structure. Besides, the fiber-based SPR biosensors offer higher sensitivity as the fine variations occurring in the vicinity of the matrix (dielectric) due to biochemical reaction will change the refractive index, and, hence, the characteristics of the surface plasmon wave [15–18]. B.B. Shuai *et al.* reported a multi-core fiber sensor based on SPR with a spectral sensitivity of about 2930 nm/RIU in the refractive index (RI) sensing range of 1.33–1.42 and, especially in the sensing range of 1.43–1.53, high linearity and sensitivity (9231.27 nm/RIU) were realized [19]. As a result, they have been applied to the detection of various biological analytes including density alteration in non-physiological cells (DANCE) [20]. T. Guo *et al.* developed an an in-fiber 12° tilted Bragg grating to detect DANCE and demonstrated an amplitude variation sensitivity of 1.8×10^4 dB/RIU, wavelength shift sensitivity of 180 nm/RIU, and a detection limit of 2×10^{-5}RIU [21].

* Corresponding authors.
E-mail addresses: zhijiesun@hrbeu.edu.cn (Z. Sun), msm-liu@126.com (C. Liu).

https://doi.org/10.1016/j.opelre.2018.01.001
1230-3402/

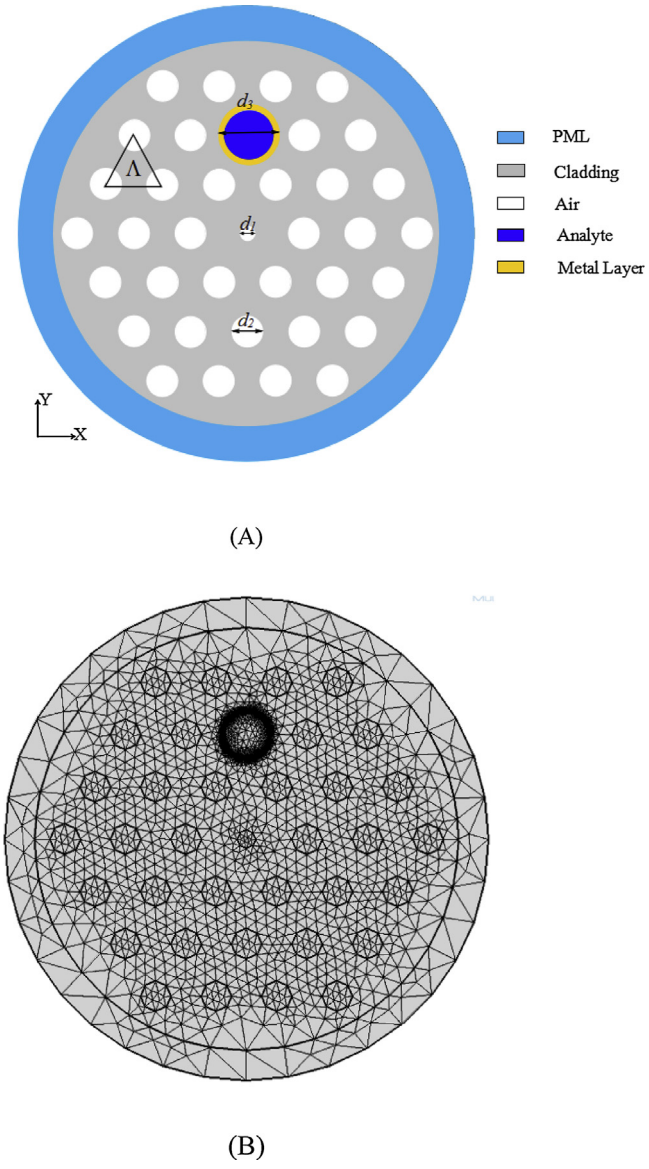

Fig. 1. (A) Cross section of the proposed PCF-SPR biosensor. (B) FEM mesh.

The study of DANCE facilitates the understanding of drug resistance, development of new drugs, separation of new subtypes from cell population, forensic analysis, and discovery of new physiological or pathological properties of cells [22]. In this paper, we describe the detection of DANCE using a PCF-SPR biosensor. Based on a numerical analysis by the finite-element method (FEM), the biosensor shows a sharp single resonance feature and high sensitivity. Human acute leukemia cells are determined by discontinuous sucrose gradient centrifugation (DSGC) in which cells are separated into several bands of S40, S50, and S6. By comparing the slight RI difference between S40, S50, and S60 (from 1.3342 to 1.3344), a wavelength shift sensitivity of 2000 nm/RIU and a detection limit of 5×10^{-5}RIU are achieved. Our analysis reveals a maximum spectral sensitivity of 9000 nm/RIU from 1.33 to 1.53, as well as high linearity corresponding to a high resolution of 1.11×10^{-5} RIU.

2. Geometry of the PCF-SPR biosensor

The cross-section of the PCF-SPR biosensor is depicted in Fig. 1(A). The biosensor comprises a central small air hole, three layers of air holes arranged in a hexagonal lattice structure, and the

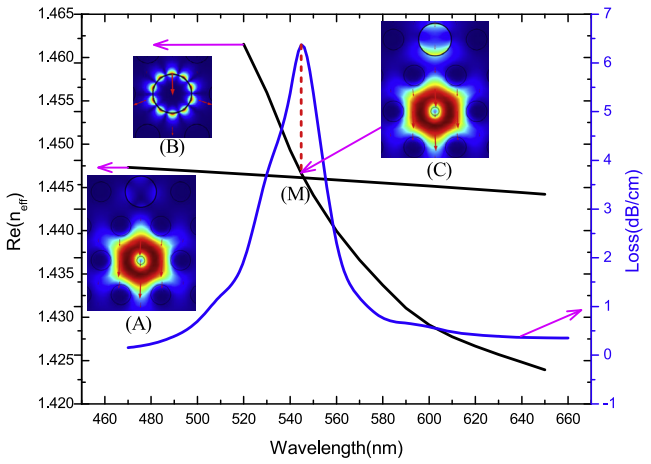

Fig. 2. Dispersion relation of the SPP mode (black), fundamental mode (pink), and loss spectrum (blue) with insets (A), (B), and (C) showing the electric field distributions at each point. Structure parameters: $d_1 = 0.2\Lambda$, $d_2 = 0.45\Lambda$, $d_3 = 0.8\ \Lambda$, and $n_a = 1.33$.

analyte channels coated with a metallized sensing layer. A small air hole at the center of the fiber core can reduce the refractive index of the core guided mode and tune the phase matching between the core-guided mode and the surface plasmon mode. This structure couples the core-guided mode and plasmonic mode at the interface of the metal layer and the analyte. The diameter of the central small air hole is $d_1 = 0.2\Lambda$, diameter of the cladding air hole is $d_2 = 0.45\Lambda$, and diameter of the analyte channel is $d_3 = 0.8\Lambda$. The pitch size of underlying hexagonal lattice is $\Lambda = 2\ \mu$m and the refractive index of the air is 1.0.

The refractive index of silica glass is given by the Sellmeier dispersion relation [23].

$$n^2 - 1 = \frac{0.6961663\lambda^2}{\lambda^2 - (0.0684043)^2} + \frac{0.4079426\lambda^2}{\lambda^2 - (0.1162414)^2} + \frac{0.897479\lambda^2}{\lambda^2 - (9.896161)^2}. \quad (1)$$

The dielectric constant of metal in the visible and near-IR region is described by the Drude model [24] as:

$$\varepsilon_{medal}(\omega) = \varepsilon_\infty - \frac{\omega_p^2}{\omega(\omega + i\omega_\tau)}, \quad (2)$$

where ω_p is the plasma frequency of metal material, ω_c is the collision frequency of electron, and $\omega = 2\pi/\lambda$, and λ represents the wavelength of the incident light in vacuum. The plasma frequency and collision frequency of some common metals are listed in Table 1.

Herein, the coupling properties of the PCF-SPR biosensor and propagation modes of electromagnetic wave are analyzed comprehensively by the finite element method (FEM) based on the use of COMSOL software [19]. Fig. 1(B) shows a typical FEM mesh along with the boundary conditions at the borders of the computed region. When the transmission loss of the core mode is used to evaluate SPR properties, a perfectly matched layer (PML) boundary condition is considered at the numerical calculation zone edges. Depending on the element order in the model, a finer or coarser mesh is required to provide the solution. The computational region is meshed into elements and the perfectly matched layer (PML) contains 1240 elements. The number of vertex of structure is 156 and the minimum element quality is equal to 0.5545.

3. Analysis and discussion

Fig. 2 shows the distribution of the refractive index of a biosensor for the analyte RI $n_a = 1.33$. The blue line presents the propagation loss of the fundamental mode effective index, whereas the black line and the pink line represent the real part of effective

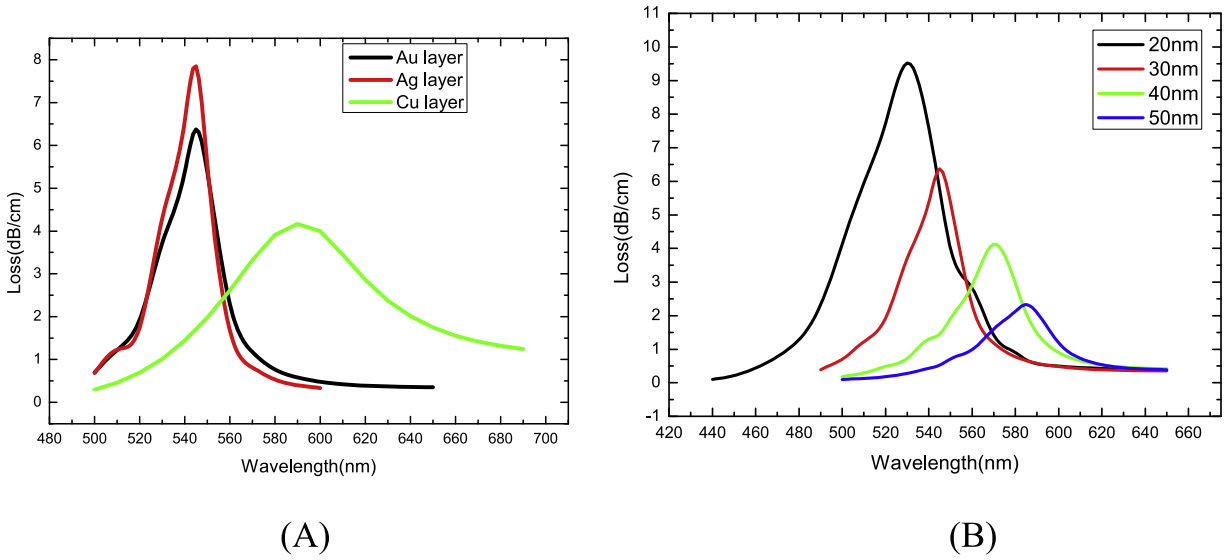

Fig. 3. Changes in the loss spectra of the plasmon peaks when the biosensor is coated with gold layers with different thicknesses. Structure parameters: $d_1 = 0.2\Lambda$, $d_2 = 0.45\Lambda$, $d_3 = 0.8\ \Lambda$, and $n_a = 1.33$.

refractive index of the fundamental mode and surface plasmon polariton (SPP) mode, respectively. The propagation loss is proportional to the imaginary part of the effective index and can be expressed as [25]:

$$\alpha_{loss} = 40\pi \cdot Im\left(n_{eff}\right) / (\ln(10)\lambda) \approx 8.686 \times k_0 \cdot Im\left(n_{eff}\right)\left(dB/m\right), \quad (3)$$

where $n_{eff} = \beta/k_0$ is the effective index of the guide mode, λ is the free-space wavelength, and $k_0 = 2\pi/\lambda$ is the vacuum wavenumber. The real part of the mode effective refractive index in the plural form shows the concept of the refractive index in the usual sense and the imaginary part describes the mode loss. Excitation of surface plasmon can be characterized by calculating the loss of the optical fiber. From point (M) in Fig. 2, a sharp loss peak is located at the resonant wavelength, 860 nm, where the dispersion relations of the fundamental mode and SPP mode intersect. The inset in Fig. 2 shows that most of the energy is transferred from the fundamental mode to SPP mode at the resonant wavelength [inset(C)], while the electric field distributions of the fundamental mode and light are confined to the fiber core and surface of the metal-coated outside the resonant wavelength [inset(A) and (B)], respectively. The energy loss of the core guided mode is mainly because excitation generates the surface plasmon mode illustrating that the core guided mode and plasma mode produce a resonance at 860 nm. Fig. 2 confirms the phase matching coupling phenomenon based on the coincidence of the loss peak and the maximum value of the fundamental mode loss spectrum can be used to locate the resonant wavelength. The modes transferred to the core of the fiber are likely to meet the phase matching condition and produce class surface plasma oscillations [26].

In this biosensor, the metal film plays an important role in the sensibility, stability, SNR, and selectivity. Fig. 3(A) shows that the loss spectra of the fundamental mode for different metal films (Au, Ag and Cu) with the same thickness (30 nm). As shown in Fig. 3(A), the silver layer exhibits the sharpest resonance peak compared with the gold and copper layers, but silver is not chemically stable and oxidized easily in practical applications. Gold not only shows larger resonance peak shifts but also is chemically stable. Therefore, a gold layer is chosen as the other active plasmonic material of the biosensor in the following analysis. The calculated results for different gold layer thicknesses from 30 nm to 50 nm are shown in Fig. 3(B). The resonance wavelength moves towards longer wavelength and the intensity of the resonance peaks decreases gradually

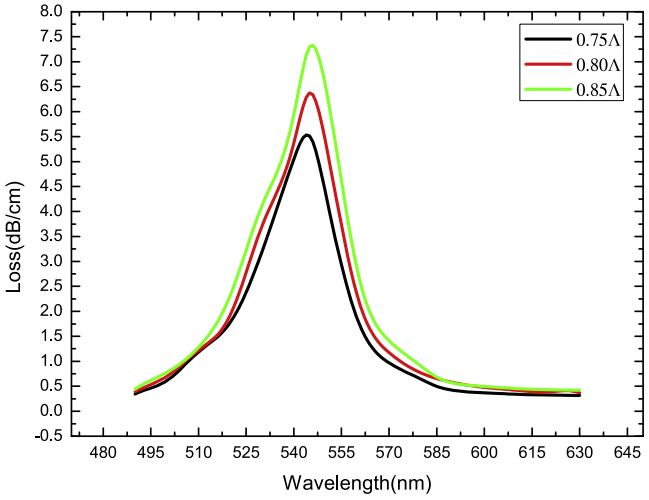

Fig. 4. Loss spectra of the fundamental mode for different diameters of the analyte channel. Structure parameters: $d_1 = 0.2\Lambda$, $d_2 = 0.45\Lambda$, and $n_a = 1.33$.

with increasing gold layer thicknesses. Since the gold layer is coated on the surface of the analyte channel, it means that more core energy is transferred to the surface plasma wave (SPW) energy, leading to stronger coupling efficiency. The increase in the overall effective index of the waveguide shifts the resonance to a longer wavelength. In addition, the resonance depth decreases while the half-width of the resonant peak and loss at the off-resonance wavelength increase with increasing gold layer thicknesses throughout the calculated thickness range.

Fig. 4 displays the loss spectra of the fundamental mode for the diameter of the analyte channel values at $d_3 = 0.75\Lambda$, 0.80Λ and 0.85Λ, respectively. The resonance wavelength is almost unchanged at 545 nm and the resonance depth increases for d_3 between 0.75 and 0.85 when all the other structural parameters are kept constant. It can be explained by that a larger analyte channel makes the metallic surface closer to the core mode. Therefore, the contact area between the mode field and metallic surface increases and more light is in turn coupled to the metallic surface, resulting in more propagation losses.

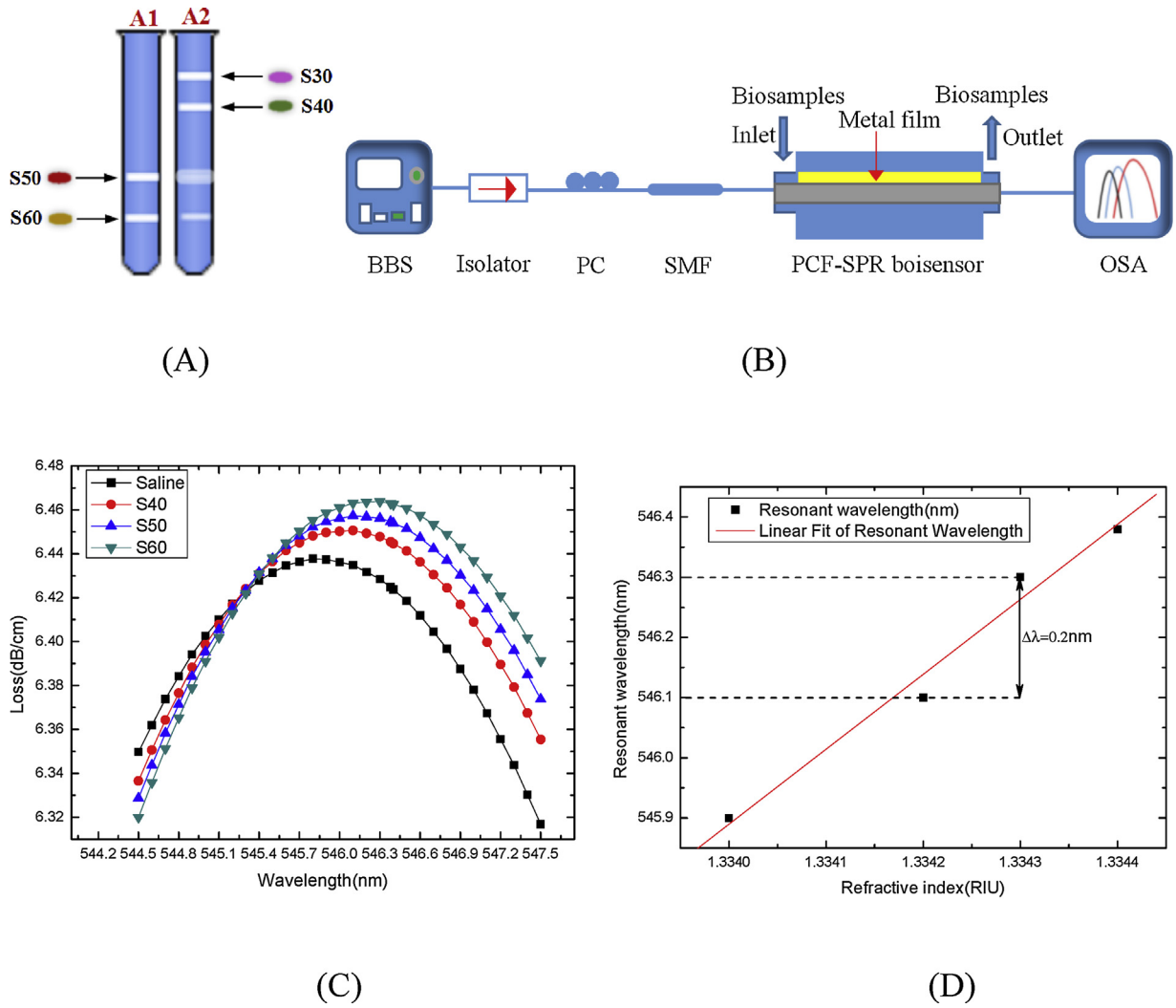

Fig. 5. (A) bio-samples (human acute leukemia cell lines, i.e., S40, S50, S60) associated with different intracellular densities separated by discontinuous sucrose gradient centrifugation (DSGC) [23]. (B) Schematic representation of the set-up. (C) Loss spectra of the fundamental mode for the biosensor for different bio-samples and (D) Linear fitting lines of the fundamental mode resonance wavelength for different samples.

4. Detection of bio-samples (human acute leukemia cells)

The phenomenon of the intracellular density change in the response of cells to drug and environmental factors is named as"density alteration in non-physiological cells" (DANCE) [22]. Fig. 5(A) illustrates that human acute leukemia cells are separated into four bands by the discontinuous sucrose gradient centrifugation (DSGC). In the A1 test tube, the cells under normal culture conditions are separated into two bands, suspending at the top of the layer of 50% and the layer of 60% sucrose as shown in Fig. 5(A). The band in DSGC is labeled as "S" with the number of sucrose concentration at which the cells are suspended. Accordingly, the layer of 50% and layer of 60% sucrose are denoted as "S50" and "S60", respectively. In the A2 test tube, the cells in "bad conditions"show two more bands at 30% and 40% sucrose layers and they were denoted as "S30" and "S40", respectively. As band S30 is not easy to culture, here we use the bands S40, S50, and S60 as the detected analytes. The experimental set-up is very simple consisting of a broadband light source (BBS), an isolator, single mode optical fiber (SMF), the PCF-SPR biosensor described above, and an optical spectrum analyzer (OSA). The schematic representation is shown in Fig. 5(B). The light from the isolator is split and coupled to the ordinary SMF through an optical connector. The light beam is input into the OSA through the PCF and a computer is used to analyze spectral data collected by the OSA to obtain the sample parameters [26]. Fig. 5 (C) shows that loss spectra of the fundamental mode of the biosensor for different cell suspensions (i.e., leukemia cells S40, S50, and S60 separated by DSGC with the same concentration of 5×10^6/ml and RI range between 1.3342 and 1.3344) and the buffer solution (saline RI 1.3340) as the control [22]. The resonance peak shifts to a longer wavelength and the resonance depth decreases gradually as shown in Fig. 5(C). The calculated results are consistent with that S60 contains "younger" leukemia cells with higher intracellular densities, while S40 carries mostly "older" ones [22]. Since absorption by the gold layer depends on the refractive index of the ambient medium, the shift in the absorption wavelength can be detected even when the change in the refractive index of the samples is very tiny [27]. Sensitivity is one of the most important parameters which can be improved by varying the refractive index of the analyte and we investigate the sensitivity of the PCF-SPR biosensor for the detection of DANCE. In the wavelength interrogation mode, variations in the refractive index of the sample can be obtained by measuring the spectral peak displacement and the spectral sensitivity S is expressed as [28]:

$$S(\lambda) = \frac{\Delta\lambda_{peak}}{\Delta n_a} \left(nm/RIU\right), \tag{4}$$

The peak shift in this work is estimated to be about $\Delta\lambda_{peak} = 0.2$ nm according to Fig. 5(D). When the variation in the analyte refractive index is $\Delta n_a = 0.0001$, the maximum spectral sensitivity of the PCF-SPR biosensor is 2000 nm/RIU for the detection of DANCE. The wavelength resolution of the detector is assumed to be $\Delta\lambda_{\min} = 0.1nm$ and the refractive index resolution of the biosensor can be defined as [29]:

$$R = \Delta n_a \Delta\lambda_{\min} / \Delta\lambda_{peak}. \quad (5)$$

Hence, the refractive index resolution of the biosensor is estimated to be about 5×10^{-5} according to Fig. 5(D).

The corresponding linear fitting curve of the resonance wavelength in relation to refractive index of the bio-sample is presented in Fig. 5(D). The fitting formula can be expressed by:

$$\lambda\,(\mathrm{nm}) = 1245.7\mathrm{n} - 1115.89,\ 1.3340 \le \mathrm{n_a} \le 1.3344, \quad (6)$$

where λ is the resonance wavelength of the biosensor and n is the refractive index of the bio-sample. The slope of the equation reveals an average sensitivity of 1245 nm/RIU in the relevant sensing range. The adjusted R-Square value of λ is 0.989 indicating high linearity.

The biosensor not only detects tiny changes in the refractive index of the bio-samples, but also achieves a large dynamic detection range from 1.33 to 1.53. The fundamental mode loss spectra for different analytes are shown in Fig. 6 which shows that the resonance peak shifts to longer wavelength when the analyte refractive index ranges from 1.33 to 1.53. The resonance peak and depth gradually increase as the analyte refractive index increases, as well. The resonance wavelength moves towards the longer wavelength from 540 nm to 930 nm as the analyte refractive index ranges from 1.33 to 1.45, but the resonance wavelength moves from 740 nm to 1010 nm as the analyte refractive index ranges from 1.46 to 1.53, as shown in Fig. 7. We investigate the sensitivity of the PCF-SPR biosensor in the analyte refractive index range of 1.35 to 1.53. The maximum peak shift here is estimated to be about $\Delta\lambda_{\mathrm{peak}} = 90$ mn according to Fig. 7(A) and the wavelength resolution of the detector is assumed to be $\Delta\lambda_{\min} = 0.1nm$. When the variation in the analyte refractive index is $\Delta n_a = 0.01$, the maximum spectral sensitivity of the PCF-SPR biosensor is of 9000 nm/RIU for refractive indexes between 1.33 and 1.53 resulting in a resolution of 1.11×10^{-5} RIU.

One of the parameters that determine the performance of the sensor is resolution. Resolution of the bio-sensor can be improved by reducing the full-width at half-maximum (FWHM) [30]. Here, the FWHM is calculated to investigate the loss spectra width, as shown in Eq. (7),

$$FWHM - \frac{1}{2} \times \left(\theta_{\min} + \theta_{\max}\right), \quad (7)$$

where $\theta_{\min}$ is the incident angle corresponding to the minimum reflected intensity, and $\theta_{\max}$ is the incident angle with the maximum reflected intensity based on the loss spectra of the fundamental mode for the biosensor. In a practical SPR sensing system, the FWHM results in not only smaller spectral deviation from the actual center of the resonant wavelength, but also suppression of the non-resonance propagation loss [29]. The FWHM and resonant losses of the fundamental mode in the sensing range of 1.33–1.53 are presented in Fig. 8. The minimum FWHM is only 10.77 nm for $n_a = 1.52$. The resonant losses of fundamental mode and SPP mode vary oppositely with increasing analyte refractive index and finally they coincide with each other [30]. The FWHM and signal-to-noise ratio (SNR) are also important parameters when evaluating sensors. This can be also demonstrated by 'figure of merit' (FOM) which can be calculated by [31]:

$$FOM = \frac{\mathrm{S}}{FWHM}, \quad (8)$$

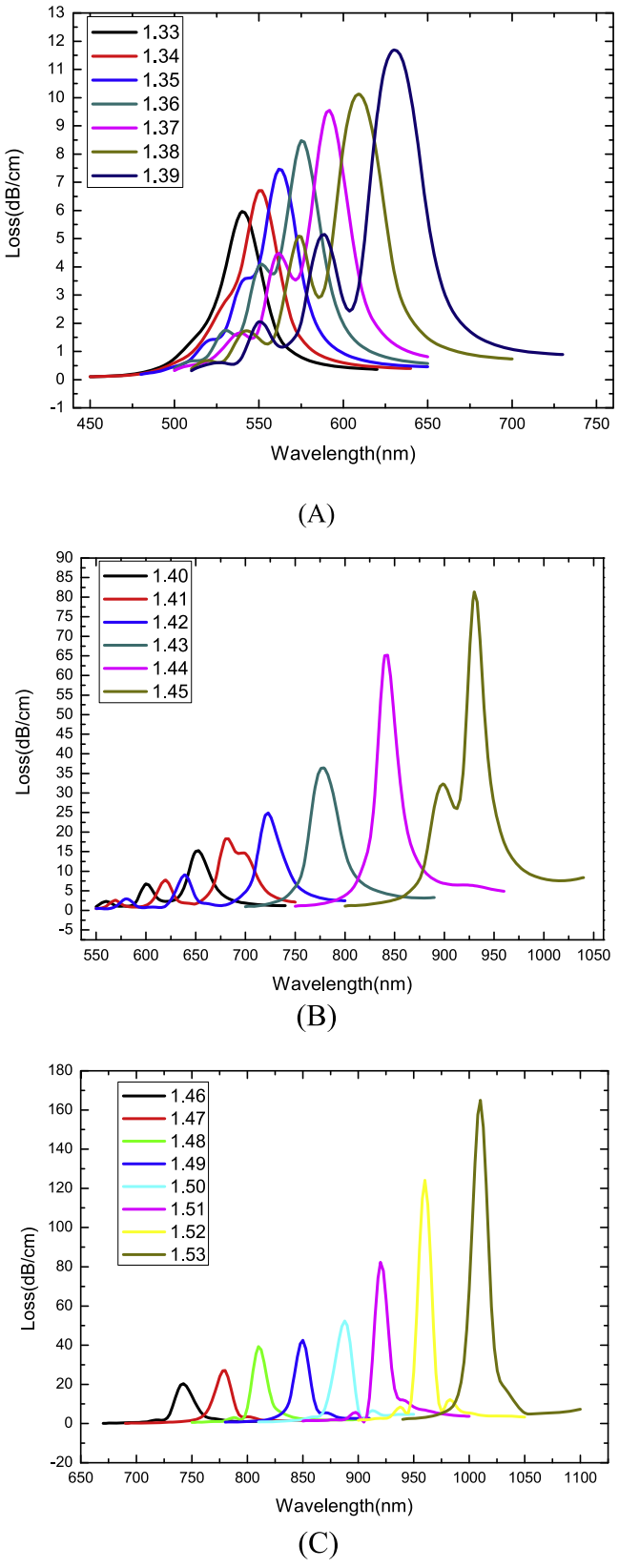

Fig. 6. Loss spectra of the fundamental mode for the biosensor for different analytes. The analyte RI varies from (A) 1.33 to 1.39, (B) 1.40 to 1.45, and (C) 1.46 to 1.53.

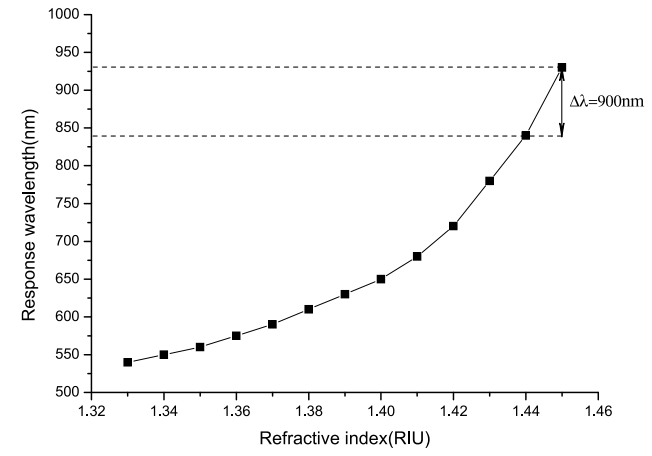

(A)

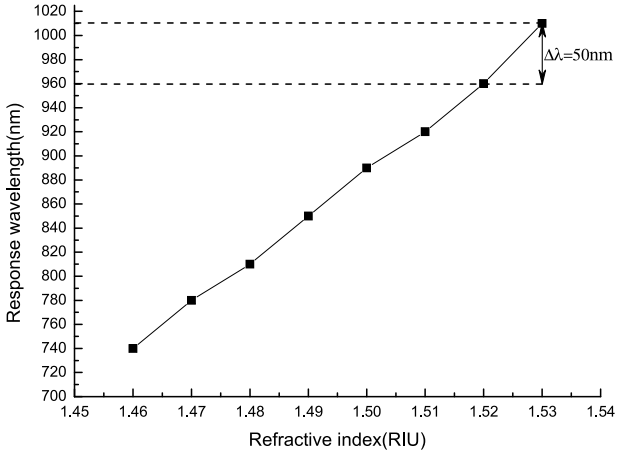

(B)

Fig. 7. (A) Fundamental mode resonance wavelength *vs.* analyte RI from 1.33 to 1.45, (B) from 1.46 to 1.53.

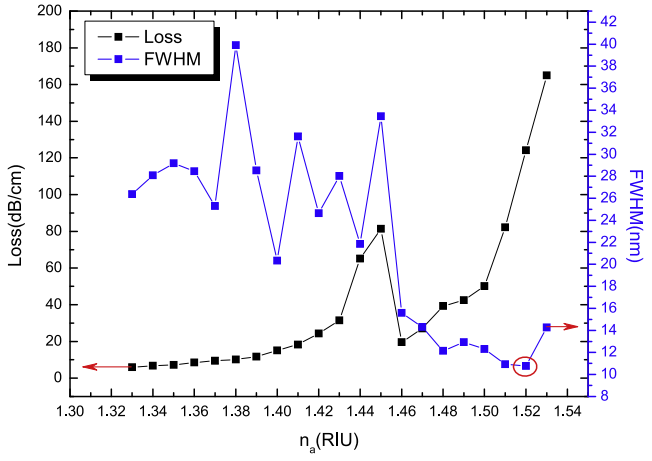

Fig. 8. Peak loss (black) of the fundamental mode for the PCF-SPR biosensor and FWHM (blue) on the analyte RI.

where S is the sensitivity, FWHM represents the full-width at half-maximum of the spectra. The estimated FOM is of 835.65 RIU^{-1}.

5. Conclusions

A PCF-SPR biosensor for the detection of the density alteration in human acute leukemia cells is described and analyzed. The coupling properties and sensing performance are numerically simulated by the finite-element method (FEM). The core guided mode effective index and surface plasma mode are sensitive to the refractive index of the analyte. In the detection of the density alteration in human acute leukemia cells, the spectral sensitivity of the PCF-SPR biosensor is of 2000 nm/RIU which is higher than the 180 nm/nm for the tilted fiber Bragg grating biosensor [21]. Moreover, a maximum spectral sensitivity of 9000 nm/RIU for analyte refractive indexes ranging from 1.33 to 1.53 and high resolution of 1.11×10^{-5} RIU are achieved. The estimated FOM is 835.65 RIU^{-1} which is higher than the 73 RIU^{-1} for PCF-SPR sensor with the selectively coated structure [32]. The PCF-SPR biosensor is an attractive solution for high-sensitivity, high-resolution, and large FOM detection of analytes with a large dynamic sensing range and applicable to biological analysis, medicine, as well as chemical and environmental monitoring.

Acknowledgements

This work jointly was supported by the National Natural Science Foundation of China [grant number 51474069]; the China Postdoctoral Science Foundation funded project [grant number 2016M591510]; the Natural Science Foundation of Heilongjiang Province [grant number E2016007]; and the City University of Hong Kong Applied Research Grant (ARG) [number 9667122].

References

[1] R.D. Harris, J.S. Wilkinson, Waveguide surface plasmon resonance sensors, Sens. Actuators. B: Chem. 29 (1995) 261–267.
[2] J. Homola, S. Yee, G. Gauglitz, Surface plasmon resonance sensors: review, Sens. Actuators. B: Chem. 54 (1) (1999) 3–15.
[3] R.C. Jorgenson, S.S. Yee, A fiber-optic chemical sensor based on surface plasmon resonance, Sens. Actuators. B: Chem. 12 (3) (1993) 213–220.
[4] R. Narayanaswamy, O.S. Wolfbeis, Optical Sensors: Industrial, Environmental, and Diagnostic Applications, Springer, New YorK, 2004.
[5] Singh Pranveer, SPR biosensors: historical perspectives and current challenges, Sens. Actuators. B: Chem. 229 (2016) 110–130.
[6] C.A. Wartchow, F. Podlaski, S. Li, K. Rowan, X. Zhang, D. Mark, K.S. Huang, Biosensor-based small molecule fragment screening with biolayer interferometry, J. Comput. Aided Mol. Des. 25 (7) (2011) 669–676.
[7] C. Ananthanawat, T. Vilaivan, V.P. Hoven, X. Su, Comparison of DNA, aminoethylglycyl PNA and pyrrolidinyl PNA as probes for detection of DNA hybridization using surface plasmon resonance technique, Biosens. Bioelectron. 25 (5) (2010) 1064–1069.
[8] O. Andreea, B. Camelia, J. Nicole, Aboul-Enein, Y. Hassan, Surface plasmon resonance (SPR) biosensors in pharmaceutical analysis, Crit. Rev. Anal. Chem. 45 (2) (2015) 97–105.
[9] E. Suenaga, H. Mizuno, Kumar K.R. Penmetcha, Monitoring influenza hemagglutinin and glycan interactions using surface plasmon resonance, Biosens. Bioelectron. 32 (1) (2012) 195–201.
[10] F. Caruso, D.N. Furlong, V. Haring, E. Rodda, DNA binding and hybridization on gold and derivatized surfaces, Sens. Actuators. B: Chem. 41 (1997) 189–197.
[11] H. Dibekkaya, Y. Saylan, F.Y. Imazb, F.Y. Imazb, Ali Derazshamshira, Surface plasmon resonance sensors for real-time detection of cyclic citrullinated peptide antibodies, J. Macromol. Sci. Part A: Pure Appl. Chem. 53 (9) (2016) 585–594.
[12] J.N. Dash, R. Jha, Graphene-based birefringent photonic crystal fiber sensor using surface plasmon resonance, IEEE Photonics Technol. Lett. 26 (11) (2014) 1092–1095.
[13] A.A. Rifat, G.A. Mahdiraji, D.M. Chow, Y.G. Shee, R. Ahmed, F.R. Adikan, Photonic crystal fiber-based surface plasmon resonance sensor with selective analyte channels and graphene-silver deposited core, Sensors 15 (5) (2015) 11499–11510.
[14] Lars Rindorf, Jesper B. Jensen, Martin Dufva, Lars Hagsholm Pedersen, Poul Erik Hiby, Ole Bang, Photonic crystal fiber long-period gratings for biochemical sensing, Virtual J. Biomed. Opt. 1 (10) (2006) 8224–8231.
[15] A. Ahmmed Rifat, et al., A novel photonic crystal fiber biosensor using surface plasmon resonance, Procedia Eng. 140 (2016) 1–7.
[16] Sarika Shukla, Navneet K. Sharma, Vivek Sajal, Sensitivity enhancement of a surface plasmon resonance based fiber optic sensor using ZnO thin film: a theoretical study, Sens. Actuators. B: Chem. 206 (2015) 463–470.

[17] H. Fu, S. Zhang, H. Chen, J. Weng, Graphene enhances the sensitivity of fiber-optic surface plasmon resonance biosensor, IEEE Sens. J. 15 (10) (2015) 5478–5482.
[18] X. Yu, Y. Zhang, S.S. Pan, P. Shum, M. Yan, Y. Leviatan, C.M. Li, A selectively coated photonic crystal fiber based surface plasmon resonance sensors, J. Opt. 12 (1) (2010) 015005–015011.
[19] B.B. Shuai, X. Li, Y.Z. Zhang, D.M. Liu, A multi-core holey fiber based plasmonic sensor with large detection range and high linearity, Opt. Express 20 (6) (2012) 5900–5974.
[20] B. Sun, M.Y. Chen, Y.K. Zhang, J.C. Yang, J.Q. Yao, H.X. Cui, Microstructured-core photonic-crystal fiber for ultra-sensitive refractive index sensing, Opt. Express 19 (5) (2011) 4091–4100.
[21] T. Guoa, F. Liua, Y. Liub, N.-K. Chenc, B.-O. Guana, J. Albertd, In-situ detection of density alteration in non-physiological cells with polarimetric tilted fiber grating sensors, Biosens. Bioelectron. 55 (2014) 452–458.
[22] Y. Liu, J.-G. Wei, B.-B. Wu, X. Wu, F.-F. Lan, Y.-C. Zhu, Density alteration in non-physiological cells, Nat. Preced. 47 (3) (2011) 533–536.
[23] A. Hassani, M. Skorobogatiy, Photonic crystal fiber-based plasmonic sensors for the detection of bio-layer thickness, J. Opt. Soc. Am. B, Opt. Phys. 26 (8) (2009) 1550–1557.
[24] M. Erdmanis, D. Viegas, M. Hautakorpi, S. Novotny, J.L. Santos, H. Ludvigsen, Comprehensive numerical analysis of a surface-plasmon-resonance sensor based on an H&HIPHEN;shaped optical fiber, Opt. Express 19 (15) (2011) 13980–13988.
[25] B. Gauvreau, A. Hassani, M.F. Fehri, A. Kabashin, M.A. Shoroobogatiy, Photonic bandgap fiber-based surface plasmon resonance sensors, Opt. Express 15 (18) (2007) 11413–11426.
[26] P.P. Zhang, J.Q. Yao, H.X. Cui, Y. Lu, A surface plasmon resonance sensor based on a multi- core photonic crystal fiber, Opt. Lett. 35 (6) (2013) 1673–1905.
[27] C. Liu, F. Wang, J. Lv, T. Sun, Q. Liu, H. Mu, P.K. Chu, Design and theoretical analysis of a photonic crystal fiber based on surface plasmon resonance sensing, J. Nanophotonics 9 (2015) 930501–9305010.
[28] Y. Zhao, Z.-Q. Deng, J. Li, Photonic crystal fiber based surface plasmon resonance chemical sensors, Sens. Actuators B: Chem. 202 (2014) 557–567.
[29] P.B. Bing, J.Q. Yao, Y. Lu, Z.Y. Li, A surface-plasmon- resonance sensor based on photonic-crystal-fiber with large size microfluidic channels, Opt. Applicata XLII 3 (2012) 450–493.
[30] A. Verma, A. Prakash, R. Tripathi, Sensitivity improvement of graphene based surface plasmon resonance biosensors with chaclogenide prism, Opt.– Int. J. Light Electron Opt. 127 (4) (2016) 1787–1791.
[31] Q. Liu, S. Li, H. Chen, J. Li, Z. Fan, High-sensitivity plasmonic temperature sensor based on photonic crystal fiber coated with nanoscale gold film, Appl. Phy. Exp. 8 (4) (2014) 046701–046706.
[32] X. Yu, S. Zhang, Y. Zhang, H.P. Ho, et al., An efficient approach for investigating surface plasmon resonance in asymmetric optical fibers based on birefringence analysis, Opt. Express 18 (17) (2010) 17950–17957.